GA–A23166

# ADVANCED TOKAMAK SCENARIO MODELING WITH OFF-AXIS ECH IN DIII–D

by
M. MURAKAMI, T.A. CASPER, L.L. LAO, H.E. ST. JOHN,
J.C. DEBOO, C.M. GREENFIELD, J.E. KINSEY, Y.R. LIN-LIU,
L.L. LODESTRO, T.C. LUCE, L.D. PEARLSTEIN, P.A. POLITZER,
R. PRATER, B.W. RICE, G.M. STAEBLER, R.D. STAMBAUGH,
E.J. STRAIT, T.S. TAYLOR, and A.D. TURNBULL

JULY 1999

## DISCLAIMER

GA–A23166

# ADVANCED TOKAMAK SCENARIO MODELING WITH OFF-AXIS ECH IN DIII–D

by
M. MURAKAMI,* T.A. CASPER,† L.L. LAO, H.E. ST. JOHN, J.C. DEBOO, C.M. GREENFIELD, J.E. KINSEY,‡ Y.R. LIN-LIU, L.L. LODESTRO,† T.C. LUCE, L.D. PEARLSTEIN,† P.A. POLITZER, R. PRATER, B.W. RICE,† G.M. STAEBLER, R.D. STAMBAUGH, E.J. STRAIT, T.S. TAYLOR, and A.D. TURNBULL

This is a preprint of a paper presented at the Twenty-Sixth European Physical Society Conference on Controlled Fusion and Plasma Physics, June 14–18, 1999 in Maastricht, The Netherlands, and to be published in *The Proceedings.*

*Oak Ridge National Laboratory, Oak Ridge, Tennessee.
†Lawrence Livermore National Laboratory, Livermore, California.
‡Oak Ridge Associated Universities, Oak Ridge, Tennessee.

Work supported by
the U.S. Department of Energy
under Contract Nos. DE-AC03-99ER54463,
W-7405-ENG-48, and DE-AC05-96OR22464

GA PROJECT 30033
JULY 1999

# Advanced Tokamak Scenario Modeling with Off-Axis ECH in DIII–D

M. Murakami,[1] T.A. Casper,[2] L.L. Lao, H.E. St. John, J.C. DeBoo, C.M. Greenfield, J.E. Kinsey,[3] Y.R. Lin-Liu, L.L. LoDestro,[2] T.C. Luce, L.D. Pearlstein,[2] P.A. Politzer, R. Prater, B.W. Rice,[2] G.M. Staebler, R.D. Stambaugh, E.J. Strait, T.S. Taylor, and A.D. Turnbull

*General Atomics, P.O. Box 85608, San Diego, California 92186-5698*

[1]*Oak Ridge National Laboratory, Oak Ridge, TN 37381, USA*
[2]*Lawrence Livermore National Laboratory, Livermore, California*
[3]*Oak Ridge Associated Universities, Oak Ridge, TN 37830, USA*

**Abstract.** Time-dependent simulations with transport coefficients derived from experimentally achieved discharges are used to explore the capability of off-axis electron cyclotron current drive (ECCD) to control hollow current profiles in negative central shear discharges. Assuming these transport coefficients remain unchanged at higher EC power levels, the simulation results show that high confinement, high normalized beta and high bootstrap fraction can be achieved with EC power expected to be available in the near future in the DIII–D tokamak.

## Introduction

In DIII–D, as in a number of tokamaks, high plasma performance has been obtained with various optimized magnetic shear configurations that exhibit an internal transport barrier (ITB). Negative central shear (NCS) discharges are created transiently during the current ramp-up by neutral beam heating and current drive. Both minimum q ($q_{min}$) and its radial location ($\rho_{q_{min}}$) decrease with time as the Ohmic current diffuses inward. In this paper we explore the ability of off-axis ECCD together with bootstrap current to control and maintain a hollow current profile. Over the next few years the EC power on DIII–D will be steadily increased from the present three-gyrotron system (1 MW per gyrotron with ~75% power delivered to plasma) to a six-gyrotron system. At the same time, an experimental effort [1] is in progress to prepare for an NCS advanced tokamak (AT) plasma demonstration with ECCD, the primary AT scenario pursued by the DIII–D program. The goal here is to achieve high normalized performance better than twice the conventional ELMing H–mode ($\beta_N H_{89P} \sim 10$) with bootstrap current fraction exceeding 50%. For a limited amount of EC power, this requires relatively high $q_{95}$ operation. The critical questions here are: (1) what are the optimal q and pressure profiles? (2) Can we sustain such optimal configurations in steady state? (3) How much power is needed to accomplish such configuration control?

Simulations are carried out using the ONETWO [2] and CORSICA [3] transport codes. The ONETWO scenario simulations, which are the primary focus in this paper, are based on transport coefficients determined from existing target discharges developed from the ongoing experiments. Measured profiles from the target discharge are used to calculate thermal diffusivities. These calculated thermal diffusivities, with the addition of the ion neoclassical diffusivity, are the baseline model diffusivities in the time-dependent transport simulations. After confirming the model with the NBI discharge, we then replaced a part of the NBI power with off-axis ECH/ECCD power. We then solved the heat and current diffusion equations consistent with fixed boundary MHD equilibrium for a fixed experimental density profile. We then extended the simulation to near steady state (typically 10 s). ECH launching angles are adjusted to sustain the high performance through bootstrap current alignment and ECCD efficiency optimization. The MHD stability of the resultant discharge is tested.

## Scenario Modeling Using Target Discharge Conditions

The recent DIII–D experimental effort has focused on transient demonstration of a discharge with the target scenario conditions using NBI alone (without ECH) [1]. This discharge is a high performance ELMing H–mode ($\beta_N$ = 3.5, $H_{89P}$ = 2.8) with divertor pumping, lasting for 0.5 s. The divertor pumping kept the density ($\bar{n}_e = 4.8\times10^{19}$ m$^{-3}$) about 20% lower than that without pumping. Figure 1 shows $T_e$, $T_i$ and $n_e$ profile of this target discharge together with calculated thermal diffusivities, $\chi_e(\rho)$ and $\chi_i(\rho)$ based on power balance analysis. We then ran the simulation with the NBI using the transport coefficients to verify the consistency of the simulation.

The EC launching direction is optimized to sustain the high performance q profile. The TORAY code [4] carries out the ray tracing for ECH power deposition and calculates the current drive by taking into account trapped electron effects. The oblique launching angle can play a significant role in ray trajectories because of the refractive effect due to the strong density gradient at the edge. Figure 2 shows normalized (local) ECCD efficiency ($\varsigma = 33\bullet n_{20} I_A R_m / P_W T_{keV}$) as a function of the minor radius of the EC resonance. The decrease in the calculated $\varsigma$ as we move further off-axis reflects the trapped electron effects. However, the experimentally measured current drive efficiency does not decrease as much with radius as calculated from theory [1,5]. In this sense, the present simulations are based on a conservative estimate of off-axis ECCD efficiency. Based on the ECCD calculation, the ONETWO code solves the current diffusion equation self-consistently with the fixed boundary equilibrium. The radial location of the current drive affects the q profile evolution by locally raising the q value which counters the trend of $q_{min}$ decreasing due to OH dissipation. ECCD maintains the required high performance sawtooth-free condition by sustaining the current required to hold $q_{min} > 1$. Figure 2 shows that higher values at $\rho$ = 0.2 and t = 4.5 s (averaged over 1 s) are obtained when ECCD is aligned somewhat inside the ITB radius where a local peak of bootstrap current resides.

The simulation with off-axis ($\rho \sim 0.5$) ECCD with 3-MW absorbed power shows that ECCD can sustain an enhanced

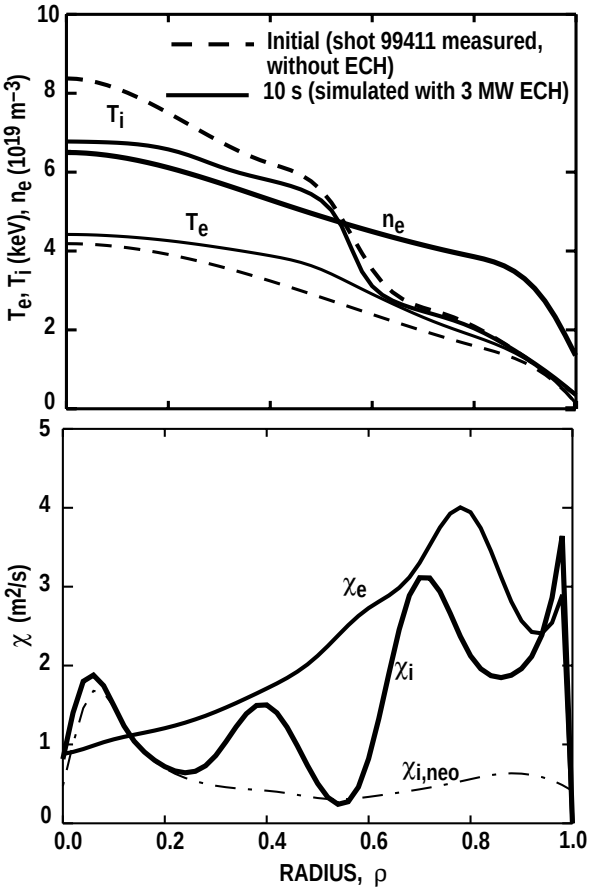


Fig.1. Initial and final electron and ion temperature profiles from the 10-s simulations using thermal diffusivities calculated from the initial (experimental) profiles.

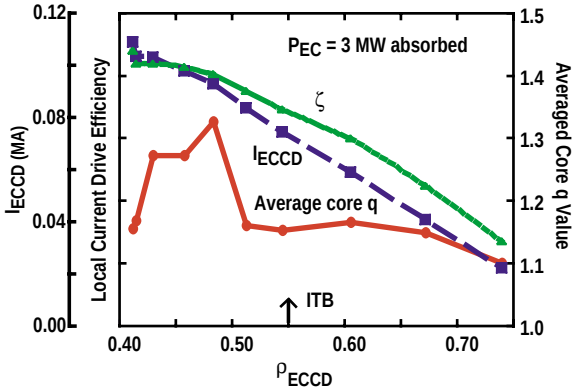


Fig. 2. Normalized (local) ECCD efficiency and averaged core q values (at $\rho$ = 0.2 and t = 4.5 s) as a function of the normalized EC resonance radius.

confinement condition at $\beta_N$ = 3.5 and $H_{89P}$ = 2.6 with bootstrap current fraction($f_{bs}$) of 55% for more than 10 s. Figure 3 shows q(ρ) and total pressure profiles at the end of the 10 s period compared with the initial state, and individual components of the current profiles for this case. Low-n MHD stability calculations show that without a conducting a wall global n = 1 pressure driven mode is strongly unstable. A conducting wall at 1.5 $a_p$ stabilizes the n = 1 mode. High-n ballooning stability calculations show both the plasma core and the edge have access to the second stability regime, and the region between ρ = 0.5 and 0.9 is below the 1st stability limit (Fig. 4). In the discharge simulation, the q(ρ) profile retains negative magnetic shear in the case for 0.5 s, and then goes toward weakly positive shear. The effects of the change of q(ρ) profiles on stability are insignificant as long as $q_{min}$ > 1.1–1.2, as shown in the two cases in Fig. 4.

Simulations were carried out with several different types of target discharges including L–mode, VH–mode (ELM-free enhanced confinement mode) as well as ELMing H–mode. When the target parameters for the simulations are different from those of the target discharges, the transport coefficients were scaled based on the ITER89P scaling expression. The results of these simulations are tabulated in Table 1, showing that fairly high performance conditions can be sustained for many confinement times with off-axis ECCD under various edge conditions.

## Theory-Based Simulations

The evolution of q(ρ) has been studied extensively with the CORSICA code [3]. The ion transport model (gyroBohm) used connects the ion thermal diffusivity to the location of $q_{min}$ and is thus sensitive to the magnetic shear. With this connection, once $\rho_{q_{min}}$ moves inward, the whole power balance is affected and results in a slow thermal collapse of the ion thermal barrier. Figure 5 shows that the duration of constant NCS barrier width, $\rho_{q_{min}}$, increases with increasing EC power in an ITB discharge with an L–mode edge. It also shows that better alignment of ECCD with the bootstrap current barrier (at ρ = 0.425 where a steep density

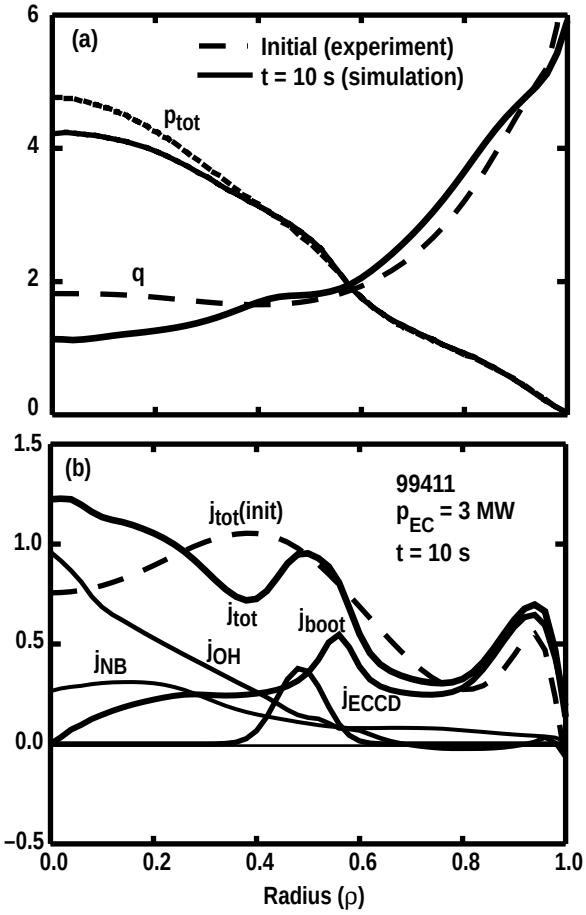


Fig. 3. Comparison of the initial and final safety factor and total pressure profiles and individual current density components.

Table 1. Parameters of NCS Scenarios With ECCD Using Different Types of Target Discharges.

| Target shot no. | 92668 | 87087 | 87087 | 99411 | 99411 |
|---|---|---|---|---|---|
| Edge condition | L | VH | VH | E-H | E-H |
| Duration (s) | 10 | 10 | 10 | 10 | 10 |
| $P_{EC}$ (MW) | 3.0 | 3.0 | 4.5 | 3.0 | 4.5 |
| $P_{FW}$ (MW) | 0 | 0 | 3.6 | 0 | 2.6 |
| $P_{NBI}$ (MW) | 6.2 | 9.2 | 4.1 | 6.2 | 2.1 |
| $I_p$ (MA) | 1.1 | 1.2 | 1.2 | 1.2 | 1.2 |
| $I_{Boot}$ (MA) | 0.59 | 0.72 | 0.84 | 0.67 | 0.81 |
| $I_{ECCD}$ (MA) | 0.18 | 0.14 | 0.20 | 0.09 | 0.17 |
| $I_{NB}$(MA) | 0.46 | 0.24 | 0.13 | 0.20 | 0.07 |
| $B_T$ (T) | 1.6 | 1.6 | 1.6 | 1.6 | 1.6 |
| $\beta_T$(%) | 3.1 | 4.6 | 5.2 | 4.3 | 4.7 |
| $\beta_N$ | 2.7 | 3.8 | 4.2 | 3.5 | 3.8 |
| $H_{89P}$ | 2.2 | 2.5 | 2.8 | 2.6 | 2.8 |
| n ($10^{20}$ $m^{-3}$) | 0.37 | 0.44 | 0.44 | 0.50 | 0.50 |
| $n/n_G$ | 0.40 | 0.44 | 0.44 | 0.50 | 0.50 |
| $T_i(0)$ (keV) | 11.2 | 10.0 | 12.4 | 6.9 | 9.0 |
| $T_e(0)$ (keV) | 5.4 | 4.5 | 6.4 | 4.5 | 6.0 |

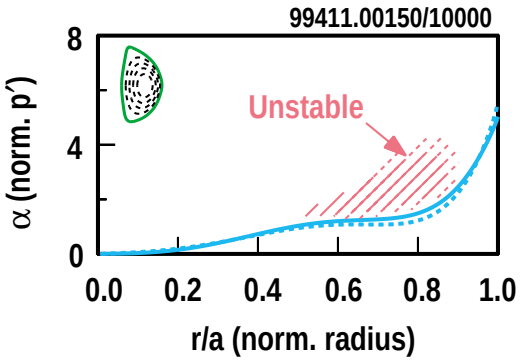


Fig. 4. Ideal ballooning stability of early (0.15 s) and final (10 s) state showing both the core and the edge have access to the second stability regime.

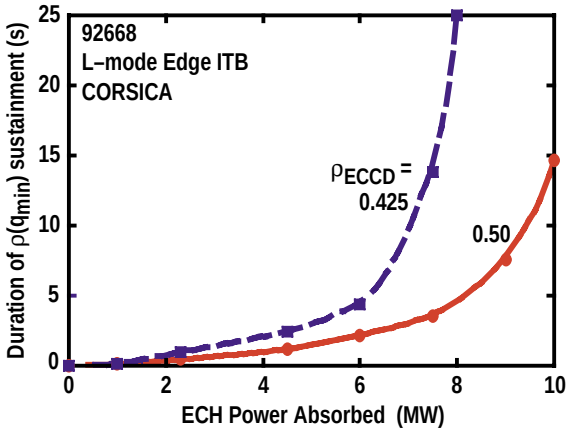


Fig. 5. Corsica simulation results on the duration of the negative central shear (or the period of constant $\rho_{q_{min}}$) as a function of the EC power for two different EC power absorption radii: ρ = 0.425 and 0.5, the former is with good bootstrap alignment.

gradient resides) reduces the power requirement to sustain the NCS. The simulations with ONETWO are qualitatively in agreement with this result, although they treat different cases.

Simulations to date have been done without including particle transport. Simulations with a broadened density profile indicate the locally enhanced bootstrap current in the barrier region further improves the ability to maintain $q_{min}$. Full exploitation of profile optimization needs a more comprehensive transport model. We are in the process of incorporating the gyro-Landau-fluid GLF23 model [6] into the ONETWO and CORSICA transport codes. This model includes magnetic shear and E×B shear effects on ion, electron, particle transport, and toroidal momentum transport. A test of the model against the experiment was done using a fast "shooting" transport code (MLT) with boundary conditions given at ρ = 0. 9 for the target discharge with the given density and rotational profiles. This test for shot 94111 shows that this model predicts well the experimental electron and ion temperature profiles.

In conclusion, time-dependent simulations based on transport coefficients derived from experimentally achieved discharges show that hollow current profiles can be maintained by combining ECCD and bootstrap current. Assuming these transport coefficients remain unchanged at higher ECH power levels, the simulation results show that high confinement, high normalized beta and high bootstrap fraction can be achieved with EC power expected to be available in the near future. However, in an earlier experiment, ECH application caused confinement degradation in an ITB discharge, and simulation efforts with theory-based models are in progress to help understand this result. Therefore, full exploitation of current profile control at high magnetic fields likely requires additional EC power planned for future years.

This is a report of work supported by the U.S. Department of Energy under Contract Nos. DE-AC03-99ER54463, DE-AC05-96OR22464, and W-7405-ENG-48.

## References

[1] T.C. Luce, this conference.

[2] H.E. St. John, et al., Plasma Phys. and Contr. Nucl. Fusion Research (Proc. 15th Int Conf. Seville, Spain), (International Atomic Energy Agency, Vienna, 1995) p. 603.

[3] T.A. Casper, et al., Proc. of the 23rd Euro. Conf. on Contr. Fusion and Plasma Phys., Kiev, Ukraine, Vol. 20C, Part I (European Physical Society, 1996) p. 295.

[4] K. Matsuda, IEEE Trans. Plasma Sci. **17**, 6 (1989).

[5] Y.R. Lin-Liu et al., this conference.

[6] R.F. Waltz, et al., Phys. Plasma **4**, 2482 (1997).

[7] C.M. Greenfield, et al., Proc. of 17th IAEA Conf., Yokahama, Japan (International Atomic Energy Agency, 1998) Paper F1-CN-61/EX5/5.